Numerical viscosity and resolution of high-order weighted essentially nonoscillatory schemes for compressible flows with high Reynolds numbers

Yong-Tao Zhang*
Department of Mathematics, University of California, Irvine, California 92697, USA

Jing Shi†
Department of Mathematics, University of Texas at Austin, Austin, Texas 78712, USA

Chi-Wang Shu‡
Division of Applied Mathematics, Brown University, Providence, Rhode Island 02912, USA

Ye Zhou§
Lawrence Livermore National Laboratory, University of California, Livermore, California 94550, USA

(Received 27 October 2002; revised manuscript received 7 July 2003; published 23 October 2003)

A quantitative study is carried out in this paper to investigate the size of numerical viscosities and the resolution power of high-order weighted essentially nonoscillatory (WENO) schemes for solving one- and two-dimensional Navier-Stokes equations for compressible gas dynamics with high Reynolds numbers. A one-dimensional shock tube problem, a one-dimensional example with parameters motivated by supernova and laser experiments, and a two-dimensional Rayleigh-Taylor instability problem are used as numerical test problems. For the two-dimensional Rayleigh-Taylor instability problem, or similar problems with small-scale structures, the details of the small structures are determined by the physical viscosity (therefore, the Reynolds number) in the Navier-Stokes equations. Thus, to obtain faithful resolution to these small-scale structures, the numerical viscosity inherent in the scheme must be small enough so that the physical viscosity dominates. A careful mesh refinement study is performed to capture the threshold mesh for full resolution, for specific Reynolds numbers, when WENO schemes of different orders of accuracy are used. It is demonstrated that high-order WENO schemes are more CPU time efficient to reach the same resolution, both for the one-dimensional and two-dimensional test problems.

DOI: 10.1103/PhysRevE.68.046709 PACS number(s): 83.85.Pt

I. INTRODUCTION

A. Preliminaries

Recently, laboratory experiments conducted on high-energy laser facilities have opened a new opportunity for experimental simulations of phenomena of interest for astrophysics, in particular the hydrodynamics of supernova explosions [1,2]. The evolution of hydrodynamic fluids for both systems is governed by the compressible Navier-Stokes equations [3,4].

The purpose of this paper is restricted to a quantitative study of the size of numerical viscosities and the resolution power of high-order weighted essentially nonoscillatory (WENO) schemes for solving one- and two-dimensional Navier-Stokes equations for compressible gas dynamics with high Reynolds numbers. We use a one-dimensional shock tube problem, a one-dimensional example motivated by supernova and laser experiments, and a two-dimensional Rayleigh-Taylor instability problem [5,6,4] as our numerical test problems. It should be noted that for the two-dimensional Rayleigh-Taylor instability problem, or similar problems with small-scale structures, the details of the small structures are determined by the physical viscosity in the Navier-Stokes equations. Thus, to obtain faithful resolution to these small-scale structures, it is essential that the numerical viscosity inherent in the scheme be small enough so that physical viscosity dominates. We consider such numerical results to be fully resolved. Results in [7] indicate that higher-order WENO schemes are more efficient in CPU time to reach the same resolution for Euler equations. In this paper, a careful mesh refinement study is performed to capture the threshold mesh related to specific Reynolds numbers for full resolution, when WENO schemes of different orders of accuracy are used to solve the Navier-Stokes equations. It is demonstrated that higher-order WENO schemes are more CPU time efficient to reach the same resolution, both for the one-dimensional (1D) and two-dimensional (2D) test problems.

We remark that there are two dimensionless parameters in the Navier-Stokes equations: the Reynolds number and the Prandtl number. The focus of this paper is on the Reynolds number since it is the most important parameter for our applications. The Reynolds number also appears in both the momentum and energy equations. Therefore, the value of the effective Reynolds number in the momentum equation controls the dissipation process that converts the eddies in the Kolmogorov scale into the heat. On the other hand, the Prandtl number appears only in the energy equation and has

*Electronic address: zyt@math.uci.edu
†Electronic address: jshi@mail.ma.utexas.edu
‡Electronic address: shu@dam.brown.edu
§Electronic address: zhou3@llnl.gov

a role on the relative energy partition. While a Prandtl number of 0.7 may be appropriate for physical application, the numerical algorithm for the governing equations does not necessarily have a fixed Prandtl number. It is, however, beyond the scope of this paper to determine the value of our effective Prandtl number for a given resolution; this will be a subject for future research. The conclusion of our paper is not affected by the determination of the effective Prandtl number.

B. Brief overview of WENO

In this paper, we compute the compressible Navier-Stokes equations in 1D and 2D, using the third-, fifth-, and ninth-order finite-difference WENO schemes, which are based on the Lax-Friedrichs building blocks and the local characteristic decompositions for the Euler terms. These WENO schemes were developed by Liu, Osher, and Chan in [8] for the third-order case, by Jiang and Shu in [9] for the fifth-order case, and by Balsara and Shu in [10] for higher-order cases. We will only give a very brief sketch of the algorithms here and refer to [9] and [10], and also to the lecture notes [11], for most of the details. For a conservation laws system

$$u_t + f(u)_x + g(u)_y = 0, \tag{1}$$

the conservative finite-difference schemes we use approximate the point values u_{ij} at a uniform (or smoothly varying) grid (x_i, y_j) in a conservative fashion. Namely, the derivative $f(u)_x$ at (x_i, y_j) is approximated along the line $y = y_j$ by a conservative flux difference

$$f(u)_x|_{x=x_i} \approx \frac{1}{\Delta x}(\hat{f}_{i+1/2} - \hat{f}_{i-1/2}),$$

where for the fifth-order WENO scheme the numerical flux $\hat{f}_{i+1/2}$ depends on the five-point values $f(u_{kj})$, $k = i-2,...,i+2$, when the wind is positive [i.e., when $f'(u) \geqslant 0$ for the scalar case, or when the corresponding eigenvalue is positive for the system case with a local characteristic decomposition]. This numerical flux $\hat{f}_{i+1/2}$ is written as a convex combination of three third-order numerical fluxes based on three different substencils of three points each, and the combination coefficients depend on a ''smoothness indicator'' measuring the smoothness of the solution in each stencil. Notice that this dimension-by-dimension approach to approximate derivatives in different directions is different from dimension splitting, and can retain high-order accuracy unlike dimension splitting. The resulting scheme can be proven uniformly fifth-order accurate in smooth regions including at any smooth extrema. For discontinuities, the solution is essentially nonoscillatory and gives sharp shock transitions. The ninth-order WENO schemes follow a similar recipe, with nine points in the stencil and five substencils of five points each. The ''monotonicity preserving limiters'' in [10] are *not* used for the test cases in this paper. For the second derivative viscous terms, we use fourth-order central difference approximations when the third- and fifth-order WENO schemes are used, and eighth-order central difference approximations when the ninth-order WENO scheme is used. Time discretization is via the third-order total variation diminishing (TVD) Runge-Kutta method in Shu and Osher [12]. The Courant-Friedrichs-Levy (CFL) number for the convective part is taken as 0.6 for all the runs, unless otherwise stated. Smaller time steps as well as higher-order time discretizations do not seem to dramatically change the conclusions drawn in this paper. All codes have been validated by first computing the Navier-Stokes equations with suitable forcing functions admitting exact, closed-form solutions, and verifying with a mesh refinement study that the correct order of accuracy is achieved.

The WENO finite-difference schemes have been chosen in this paper because they are uniformly high-order accurate and robust for strong shocks or other discontinuities, which are features especially suitable for computing high-Reynolds-number Navier-Stokes equations containing both sharp gradient regions and rich smooth solution structures. Notice that the dimension-by-dimension approach to approximate derivatives in all directions is different from dimension splitting, and can retain high-order accuracy. We present the numerical results for the one-dimensional problem in Sec. II and for the two-dimensional problem in Sec. III.

C. Measurements of resolution and convergence

We assume there are two uniform Cartesian meshes Γ_h and $\Gamma_{h/2}$, which have mesh sizes h and $h/2$ in each direction, respectively. We further assume that the grid points $\{x_i^h,\ i = 1,2,...\}$ of the coarse mesh Γ_h are also the grid points of the fine mesh $\Gamma_{h/2}$, i.e., $\{x_i^h,\ i = 1,2,...\} \subset \{x_i^{h/2},\ i = 1,2,...\}$. This assumption is not essential but it does allow us to measure the asymptotic error $E_{h,i}$ below without using interpolation. We denote u_h and $u_{h/2}$ to be the numerical solutions of our r-order WENO schemes on the two meshes Γ_h and $\Gamma_{h/2}$, respectively, and u to be the exact solution of our partial differential equation. The error at each grid point is $e_{h,i} = u_{h,i} - u_i$ and $e_{h/2,i} = u_{h/2,i} - u_i$. When u is smooth, we have $e_{h,i} \approx Ch^r$ and $e_{h/2,i} \approx 2^{-r}Ch^r$.

Definition 1.1. The asymptotic convergence error at a grid point x_i of Γ_h (which is also a grid point of the more refined mesh $\Gamma_{h/2}$) is defined by

$$E_{h,i} \triangleq u_{h,i} - u_{h/2,i}.$$

It is easy to see $E_{h,i} \approx (1-2^{-r})e_{h,i}$ for a smooth solution u. The L^1 and L^∞ asymptotic convergence errors in a region Ω are defined as

$$\|E_h\|_{L^1(\Omega)} = \frac{1}{N}\sum_{i=1}^{N} |E_{h,i}|, \quad \|E_h\|_{L^\infty(\Omega)} = \max_{1 \leqslant i \leqslant N} |E_{h,i}|,$$

where N is the number of grid points within Ω in the coarser mesh Γ_h.

Note that when the solution u is smooth, the asymptotic convergence error $\|E_h\|$ is $1-2^{-r}$ times the size of the numerical error $\|e_h\|$ on the coarser mesh for an r-order numerical scheme. It is obvious that the numerical order of accuracy of the scheme is given approximately by

$$r=\frac{\log(\|E_h\|/\|E_{h/2}\|)}{\log 2}.$$

Definition 1.2. Given $\varepsilon>0$, a numerical solution for the nondimensional Navier-Stokes equations is considered resolved on the ε level in domain Ω with respect to the norm $\|\cdot\|$ if

$$\|E_h\|_\Omega \leqslant \varepsilon,$$

where E_h measures the asymptotic convergence error, defined above, of the density ρ.

In our one- and two-dimensional numerical examples, discontinuous initial conditions are used. In order to make it possible for the numerical viscosity of the WENO schemes to be smaller than the physical viscosity when the mesh size is suitably small, we smooth the discontinuous initial condition to be continuous but have a narrow transition region. For example, if the initial condition is a step function,

$$f(x)=\begin{cases} a, & x<x_0, \\ b, & x\geqslant x_0, \end{cases} \tag{2}$$

then the smoothed initial condition will be

$$f(x)=\frac{b-a}{2}\tanh[n(x-x_0)]+\frac{b+a}{2}, \tag{3}$$

where n determines the width of the transition region. The bigger n is, the narrower the transition region becomes.

Finally, we define a quantitative measurement for the difference of two different numerical solutions, $\{u_i\}_{i=1}^m$ and $\{v_i\}_{i=1}^n$, on two grids. These two grids can be the same or different. When they are different, one can be a subset of the other, or they can be totally different.

Definition 1.3. $\{u_i\}_{i=1}^m$ and $\{v_i\}_{i=1}^n$ are numerical solutions on meshes Γ_m and Γ_n of domain Ω, grid point number $n>m$. $\{\Pi v_i\}_{i=1}^m$ is the high-order ENO interpolation of $\{v_i\}_{i=1}^n$ from the finer mesh Γ_n to the coarser mesh Γ_m, if necessary. The L^1 absolute difference between u and v is defined as

$$\|E_h\|_{L^1(\Omega)}=\frac{1}{m}\sum_{i=1}^m |u_i-\Pi v_i|.$$

The L^1 relative difference between u and v is defined as

$$\|E_r\|_{L^1(\Omega)}=\frac{1}{m}\sum_{i=1}^m \left|\frac{u_i-\Pi v_i}{u_i}\right|,$$

where we assume $u_i\neq 0$, $i=1,...,m$. The L^1 visual relative difference between u and v is defined as

$$\|E_v\|_{L^1(\Omega)}=\frac{\frac{1}{m}\sum_{i=1}^m |u_i-\Pi v_i|}{\max_{1\leqslant i\leqslant m} u_i-\min_{1\leqslant i\leqslant m} u_i},$$

where we assume $\max_{1\leqslant i\leqslant m} u_i\neq\min_{1\leqslant i\leqslant m} u_i$.

II. THE ONE-DIMENSIONAL PROBLEM

First we nondimensionalize the Navier-Stokes equations. The actual computation is performed in the nondimensionalized quantities. Nondimensionalization is conducted with the same notation as that used in Ryutov *et al.* [13]. Denote the length x scale by a cm, the density ρ scale by b g/cm^3, and the pressure p scale by c dyn/cm^2. Then the time t scale is $a\sqrt{b/c}$ and the velocity u scale is $\sqrt{c/b}$. Taking $\bar{x}=x/a$, $\bar{\rho}=\rho/b$, $\bar{p}=p/c$, $\bar{t}=t/(a\sqrt{b/c})$, $\bar{u}=u/\sqrt{c/b}$, and omitting bars for the scaled variables, we obtain the nondimensionalized Navier-Stokes equations in 1D,

$$\rho_t+(\rho u)_x=0,$$

$$(\rho u)_t+(\rho u^2+p)_x=\frac{1}{\mathrm{Re}}(\tfrac{4}{3}u_{xx}), \tag{4}$$

$$E_t+[u(E+p)]_x=\frac{1}{\mathrm{Re}}\left[\frac{2}{3}(u^2)_{xx}+\frac{1}{(\gamma-1)\mathrm{Pr}}(C^2)_{xx}\right].$$

Here E is the total energy, $E=[p/(\gamma-1)]+\frac{1}{2}\rho u^2$, where γ is the ratio of specific heats, with $\gamma=1.4$ for air. Pr is the Prandtl number, with Pr$=0.7$. C is the sound speed, related to the pressure p and the density ρ by $C^2=\gamma p/\rho$. Re is the Reynolds number,

$$\mathrm{Re}=\frac{a\sqrt{c/b}}{\nu}, \tag{5}$$

where ν is the kinematic viscosity, which is related to the dynamic viscosity μ by

$$\nu=\frac{\mu}{\rho}. \tag{6}$$

A. WENO computation for the Navier-Stokes equations on a shock tube problem

We first solve Sod's one-dimensional shock tube problem for the Navier-Stokes equations (4). The computational domain is $[-1.2,1.2]$. The Riemann initial condition is given by

$$(\rho,u,p)=\begin{cases} (1,0,1), & x\leqslant 0 \\ (0.125,0,0.1), & x>0 \end{cases} \tag{7}$$

smoothed out by Eq. (3) with $n=10$ as our smoothed initial condition. Final simulation time is $t=0.4$. WENO3, WENO5, and WENO9 (third-, fifth-, and ninth-order WENO schemes) are used. Reynolds numbers are taken to be Re $=1000$, 5000, and 10 000.

In Table I, we list the L^1 and L^∞ asymptotic convergence errors and numerical orders of accuracy (see definition 1.1) for WENO3 and WENO5 schemes when the Reynolds number Re$=1000$. The results for WENO9 follow similar patterns and are thus omitted to save space. We also present the same errors and orders when the Reynolds number Re $=10\,000$ in Table II. The results for Re$=5000$ are similar and hence are omitted to save space. We can clearly see that the

TABLE I. Asymptotic convergence errors and numerical orders of accuracy for WENO3 and WENO5; Reynolds number=1000; Sod's shock tube problem.

		WENO3		
N	L^1 error	Order	L^∞ error	Order
100	9.94×10^{-4}		1.34×10^{-2}	
200	2.99×10^{-4}	1.73	6.44×10^{-3}	1.05
400	6.54×10^{-5}	2.19	1.77×10^{-3}	1.86
800	9.24×10^{-6}	2.82	3.10×10^{-4}	2.51
1600	1.06×10^{-6}	3.12	3.94×10^{-5}	2.98
		WENO5		
N	L^1 error	Order	L^∞ error	Order
100	3.50×10^{-4}		8.63×10^{-3}	
200	5.10×10^{-5}	2.78	2.43×10^{-3}	1.83
400	3.39×10^{-6}	3.91	2.38×10^{-4}	3.35
800	1.29×10^{-7}	4.72	1.04×10^{-5}	4.52
1600	5.14×10^{-9}	4.65	3.70×10^{-7}	4.81

numerical orders of accuracy approach the theoretically designed orders when the mesh is refined, as expected. However, for larger Reynolds numbers, more grid points are required before we can see the numerical orders of accuracy approaching the theoretical value. On the other hand, we could ask the question of the number of grid points required to achieve a fixed ε resolution, see definition 1.2. Notice that this is different from the question of asymptotic errors and orders but is, however, a more practical question since it is directly related to the CPU cost of the algorithm to reach a fixed resolution. The grid point numbers N which are needed to get a resolved solution on the $\varepsilon=10^{-4}$ level with respect to the L^∞ norm on the whole domain $\Omega=[-1.2,1.2]$ for WENO3, WENO5, and WENO9 are listed in Table III. In Fig. 1, we plot the relationship of the Reynolds number and the threshold mesh point number N for this resolution. We can conclude the relationship is almost linear, and the number of grid points needed to reach this resolution for WENO9 is about one-half that for WENO5, which in turn is about one-half that for WENO3.

TABLE II. Asymptotic convergence errors and numerical orders of accuracy for WENO3 and WENO5; Reynolds number $=10\,000$; Sod's shock tube problem.

		WENO3		
N	L^1 error	Order	L^∞ error	Order
2000	3.30×10^{-5}		8.33×10^{-3}	
4000	1.00×10^{-5}	1.72	2.76×10^{-3}	1.59
8000	1.70×10^{-6}	2.56	5.79×10^{-4}	2.25
16 000	2.04×10^{-7}	3.06	7.69×10^{-5}	2.91
		WENO5		
N	L^1 error	Order	L^∞ error	Order
1000	4.49×10^{-5}		1.31×10^{-2}	
2000	1.08×10^{-5}	2.06	4.69×10^{-3}	1.49
4000	7.94×10^{-7}	3.77	4.89×10^{-4}	3.26
8000	3.41×10^{-8}	4.54	2.20×10^{-5}	4.48

TABLE III. Grid point number N needed to obtain resolved solutions with L^∞ asymptotic convergence error $<10^{-4}$ on the domain $[-1.2,1.2]$. Shock tube problem.

Reynolds no.	N of WENO3	N of WENO5	N of WENO9
1000	1600	800	400
5000	8000	4000	2000
10 000	16 000	8000	4000

Next, we compare the number of grid points needed to resolve in three different regions, namely the rarefaction wave, the contact discontinuity, and the shock wave region for the shock tube problem with Re=1000. The L^∞ asymptotic convergence error and orders of convergence for WENO5 are computed at three different regions, namely the rarefaction wave region $[-0.7,0.1]$, the contact discontinuity region $[0.2,0.52]$, and the shock wave region $[0.6,0.8]$. From the results in Table IV, we can conclude that for the same grid point number, the asymptotic convergence error in the rarefaction wave region is much smaller than that in the contact discontinuity region, which in turn is much smaller than that in the shock wave region, In this problem, for WENO5, $N=800$ points are needed to resolve the shock wave region on the 10^{-4} level with respect to the L^∞ norm, while only $N=200$ points are needed to resolve the contact discontinuity region and only $N=100$ points are needed to resolve the rarefaction wave to the same level of resolution. The conclusion is that, for the Navier-Stokes equations with high Reynolds numbers, the rarefaction wave is the easiest to resolve,

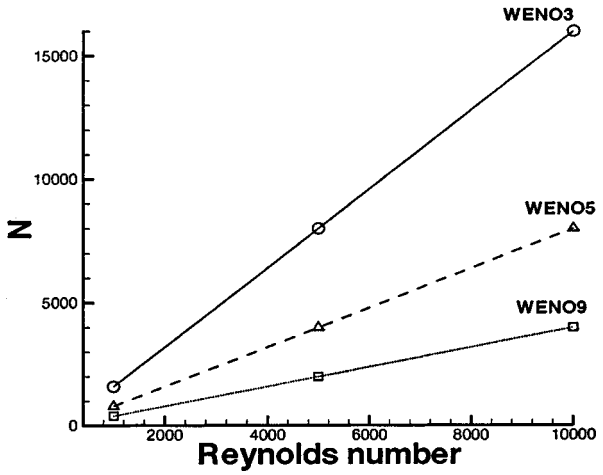

FIG. 1. The relationship of the Reynolds number and the number of mesh points needed to obtain resolved solutions with L^∞ convergence error $<10^{-4}$ on the domain $[-1.2,1.2]$. Shock tube problem. The x axis is the Reynolds numbers and the y axis is the threshold number of grid points that WENO uses to obtain 10^{-4}-resolved solutions. The solid line with circles is for the third-order WENO; the dashed line with triangles is for the fifth-order WENO; the dotted line with squares is for the ninth-order WENO.

TABLE IV. Asymptotic convergence errors and numerical orders of accuracy for WENO5 at different regions: the rarefaction wave region $[-0.7, 0.1]$, the contact discontinuity region [0.2,0.52], and the shock wave region [0.6,0.8]. Reynolds number=1000; Sod's shock tube problem.

	Rarefaction		Contact		Shock	
N	L^∞ error	Order	L^∞ error	Order	L^∞ error	Order
50	6.64×10^{-4}		1.40×10^{-3}		1.82×10^{-2}	
100	5.54×10^{-5}	3.58	1.65×10^{-4}	3.09	8.63×10^{-3}	1.08
200	2.03×10^{-6}	4.77	4.17×10^{-5}	1.98	2.43×10^{-3}	1.83
400	6.58×10^{-8}	4.94	1.59×10^{-6}	4.71	2.38×10^{-4}	3.35
800	2.08×10^{-9}	4.98	5.61×10^{-8}	4.83	1.04×10^{-5}	4.52
1600	6.09×10^{-11}	5.09	1.83×10^{-9}	4.94	3.70×10^{-7}	4.81

the shock wave is the hardest to resolve, and contact discontinuity is in between in terms of difficulties for resolution.

B. WENO computation for the Navier-Stokes equations with Reynolds numbers corresponding to the supernova and the laser experiments

The objective of this subsection is to simulate the Navier-Stokes equations with Reynolds numbers corresponding to the supernova and the laser experiments, respectively. WENO schemes with adequately refined meshes for a reliable resolution are used. Since the supernova and the laser experiments should yield identical results under the scaling when the Euler equations are used, we would like to see the effect of different physical viscosities corresponding to the supernova and to the laser experiments. We emphasize that this is a one-dimensional model and does not take spherical geometry into consideration, however we do expect the essential conclusions about numerical viscosity, resolution, and convergence in this simple model to give important guidance to the real physical problems.

We take the initial condition ρ (in g/cm^3), velocity u (in cm/ms), and pressure p (in Mbar) from the data at $t=2$ ns in Drake *et al.* [14], kindly provided to us by Omar Hurricane. See Fig. 2 for the plot of density and pressure.

The dimensional computational domain is $0\leqslant x\leqslant 0.095$ in centimeters. We nondimensionalize the data by $\bar{x}=x/a$ with $a=0.01$ cm, $\bar{\rho}=\rho/b$ with $b=1$ g/cm^3, and $\bar{p}=p/c$ with $c=50$ Mbar. Then the time t is scaled by $\bar{t}=t/(a\sqrt{b/c})$ and the velocity u is scaled by $\bar{u}=u/\sqrt{c/b}$. We compute the nondimensionalized Navier-Stokes equations (4) on these nondimensionalized data to nondimensionalized times $\bar{t}=4$ ns$/(a\sqrt{b/c})$ and $\bar{t}=6$ ns$/(a\sqrt{b/c})$. We omit the bars for the scaled variables in the following.

On the left boundary $x=0$, we use a characteristic boundary condition because the left boundary is not really an outflow boundary. On the right boundary $x=9.5$, we use a Neumann boundary condition because it is an outflow boundary.

In this subsection, we use the fifth-order finite difference WENO scheme [9] with uniform meshes. Since the original data are on a nonuniform mesh, we use a fourth-order ENO interpolation to obtain initial conditions on our mesh from the given data.

Our one-dimensional example is motivated by the supernova and laser experiments. The Reynolds numbers are estimated to be (Ryutov *et al.* [13] and Robey *et al.* [15])

$$\mathrm{Re}=1.9\times10^{11} \quad \text{for the supernova,}$$

$$\mathrm{Re}=1.4\times10^{5} \quad \text{for the laser experiments.}$$

The cases corresponding to these Reynolds numbers will be called Supernova and Laser, respectively. One must note that other laser experiments may have different Reynolds numbers.

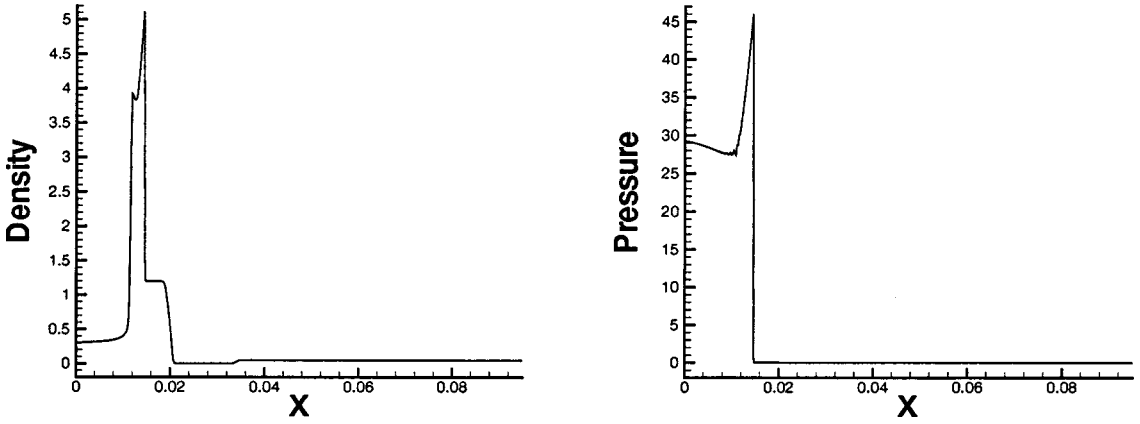

FIG. 2. Dimensional initial data at time $t=2$ ns. Left: density ρ (in g/cm^3); right: pressure p (in Mbar).

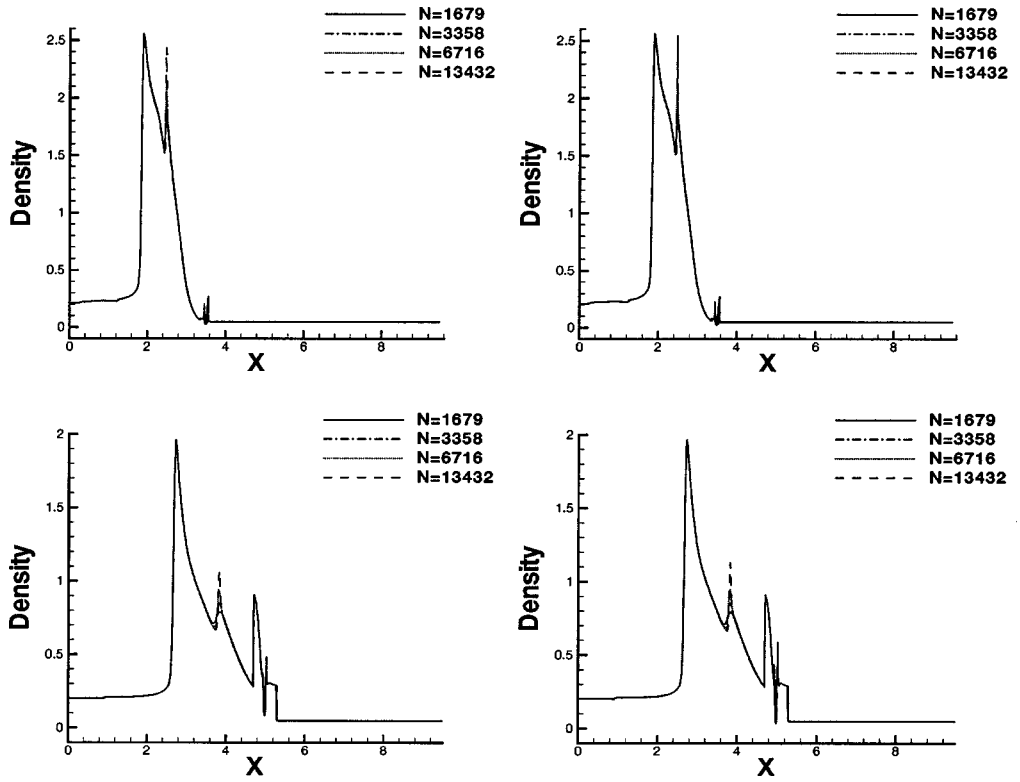

FIG. 3. The fifth-order WENO solution with $N=1679$ grid points (the solid line), 3358 grid points (the dash-dotted line), 6716 grid points (the dotted line), and 13 432 grid points (the dashed line). Left: results of Laser; right: results of Supernova. Density ρ. Top: at time $\bar{t}=4$ ns/$(a\sqrt{b/c})$; bottom: at time $\bar{t}=6$ ns/$(a\sqrt{b/c})$, where $a=0.01$ cm, $b=1$ g/cm^3, and $c=50$ Mbar.

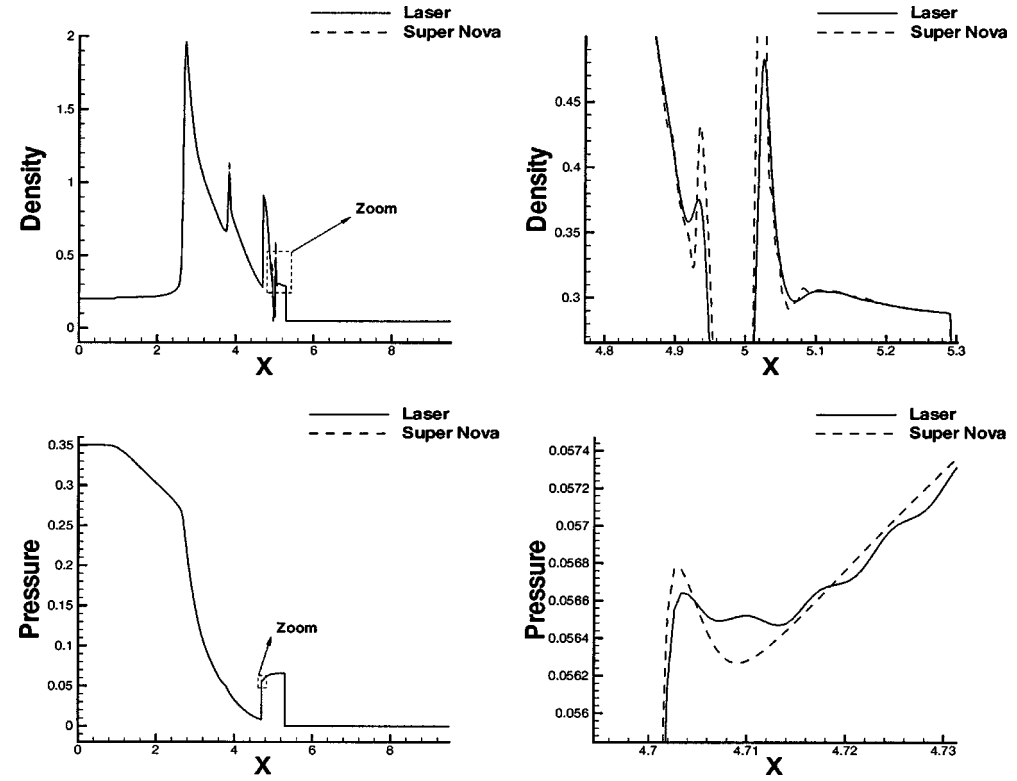

FIG. 4. Overlay of fifth-order WENO solutions of Laser and Supernova with 13 432 grid points. Laser (the solid line) vs Supernova (the dashed line). Left: the whole picture; right: enlarged region. Top: density ρ; bottom: pressure p. Time $\bar{t}=6$ ns/$(a\sqrt{b/c})$, where $a=0.01$ cm, $b=1$ g/cm^3, and $c=50$ Mbar.

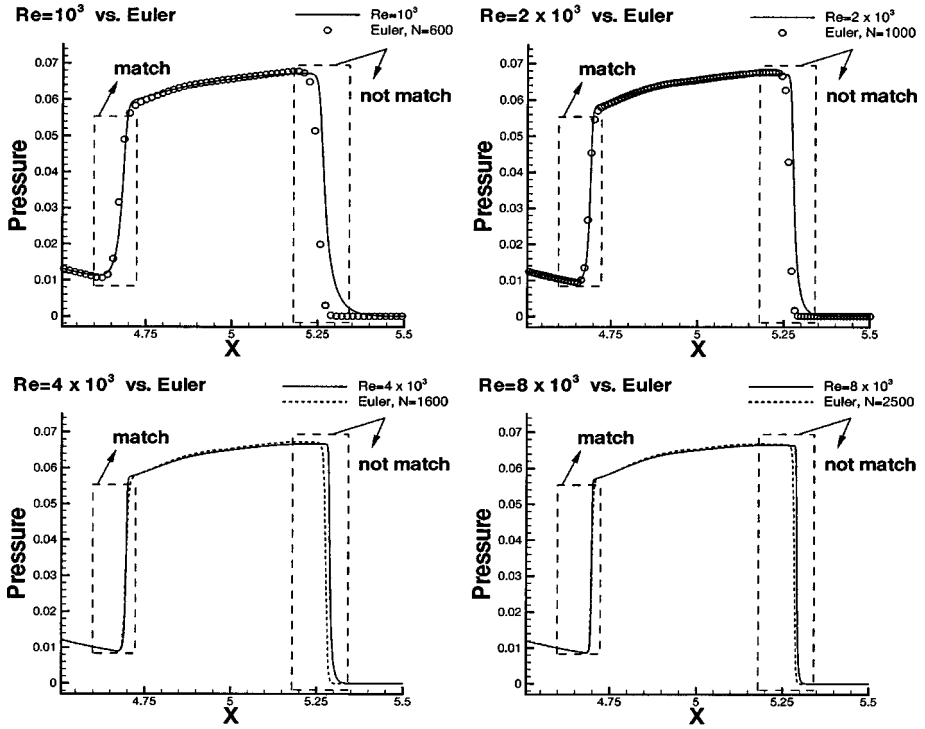

FIG. 5. Fifth-order WENO solutions of Euler with different N matching converged solutions of the Navier-Stokes equations with different Reynolds numbers. Pressure p, the shock region. Top left: NS with $\mathrm{Re}=10^3$ matching Euler with $N=600$; top right: NS with $\mathrm{Re}=2\times10^3$ matching Euler with $N=1000$; bottom left: NS with $\mathrm{Re}=4\times10^3$ matching Euler with $N=1600$; bottom right: NS with $\mathrm{Re}=8\times10^3$ matching Euler with $N=2500$. Solid lines are for NS, dashed lines or circles are for Euler. Time $\bar{t}=6\ \mathrm{ns}/(a\sqrt{b/c})$, where $a=0.01$ cm, $b=1\ \mathrm{g/cm^3}$, and $c=50$ Mbar.

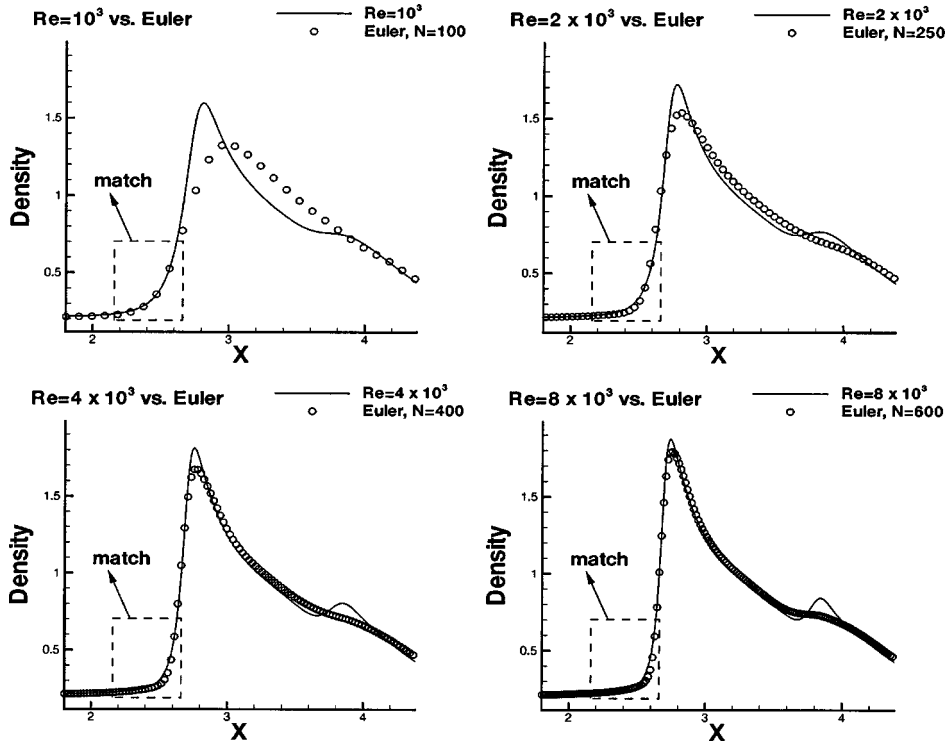

FIG. 6. Fifth-order WENO solutions of Euler with different N matching converged solutions of the Navier-Stokes equations with different Reynolds numbers. Density ρ, the contact discontinuity region. Top left: NS with $\mathrm{Re}=10^3$ matching Euler with $N=100$; top right: NS with $\mathrm{Re}=2\times10^3$ matching Euler with $N=250$; bottom left: NS with $\mathrm{Re}=4\times10^3$ matching Euler with $N=400$; bottom right: NS with $\mathrm{Re}=8\times10^3$ matching Euler with $N=600$. Solid lines are for NS, circles are for Euler. Time $\bar{t}=6\ \mathrm{ns}/(a\sqrt{b/c})$, where $a=0.01$ cm, $b=1\ \mathrm{g/cm^3}$, and $c=50$ Mbar.

TABLE V. Physical viscosity versus numerical viscosity, in the shock region. *A*, number of points *N* for WENO9; *B*, number of points *N* for WENO5; *C*, number of points *N* for WENO3.

Reynolds no.	*A*	*B*	*C*
1000	400	600	1000
2000	600	1000	1600
4000	1000	1600	2500
8000	1600	2500	4500

TABLE VI. Physical viscosity versus numerical viscosity, in the contact discontinuity region. *A*, number of points *N* for WENO9; *B*, number of points *N* for WENO5; *C*, number of points *N* for WENO3.

Reynolds no.	*A*	*B*	*C*
1000	70	100	250
2000	100	250	400
4000	200	400	800
8000	300	600	1200

We can look at the convergence of the WENO schemes by comparing the simulation results using $N=1679$, 3358, 6716, and 13 432 uniform mesh points in Fig. 3 for $\bar{t}=4\ \mathrm{ns}/(a\sqrt{b/c})$ and for $\bar{t}=6\ \mathrm{ns}/(a\sqrt{b/c})$ (only density is shown to save space), where $a=0.01$ cm, $b=1\ \mathrm{g/cm^3}$, and $c=50$ Mbar. It is clear that on this scale, even the coarsest mesh gives adequate resolution in most parts of the domain, with the more refined meshes giving better resolutions near sharp gradient regions. On a more quantitative level, the L^1 asymptotic convergence error of the numerical solutions between the two meshes with $N=6716$ and 13 432 points (see definition 1.1) is less than 1.9×10^{-3}, the L^1 relative difference is less than 4.2×10^{-3}, and the L^1 visual relative difference is less than 9.6×10^{-4} for the density ρ at both $\bar{t}$. The L^1 differences for the velocity u and for the pressure p are on similar levels. This gives us confidence that the most refined mesh calculation is a numerically converged, or more precisely at least 10^{-3}-resolved solution for the Navier-Stokes equations for those Reynolds numbers.

Next, we use the numerically converged solutions to look at the difference between Laser and Supernova. We plot the results using the most refined 13 432 mesh points of Laser and Supernova in the same graph. See Fig. 4 for the density and pressure at $\bar{t}=6\ \mathrm{ns}/(a\sqrt{b/c})$. The velocity at this time and all quantities at $\bar{t}=4\ \mathrm{ns}/(a\sqrt{b/c})$ are not shown to save space, as they present similar patterns. The difference between the results for Laser and Supernova is very small but still discernible, especially when enlarged at the place of rich structures; see the graphs at the right in Fig. 4. On a more quantitative level, the L^1 absolute difference of density ρ in the enlarged region between the Laser and Supernova cases (the upper-right graph in Fig. 4) is 1.8×10^{-2}, the L^1 relative difference is 9.6×10^{-2}, and the L^1 visual relative difference is 3.4×10^{-2}, all of them being more than a magnitude larger than the 10^{-3} resolution of the numerical solutions, hence they are not due to numerical errors but are true differences of solutions to the Navier-Stokes equations with different Reynolds numbers. The same conclusion also holds for the velocity u and for the pressure p. This indicates that there are indeed small but discernible differences between the solutions of the Navier-Stokes equations with Reynolds numbers corresponding to the Supernova and to the Laser experiment. These differences are most prominent near the high gradient regions in the solutions (the enlarged regions). Depending on whether such differences are significant or not for the physical phenomena to be studied, the laser experiment may or may not be a suitable model to study supernova.

C. Study of numerical viscosity of WENO schemes

The objective of this subsection is to perform a quantitative study on the size of the numerical viscosity of the third-,

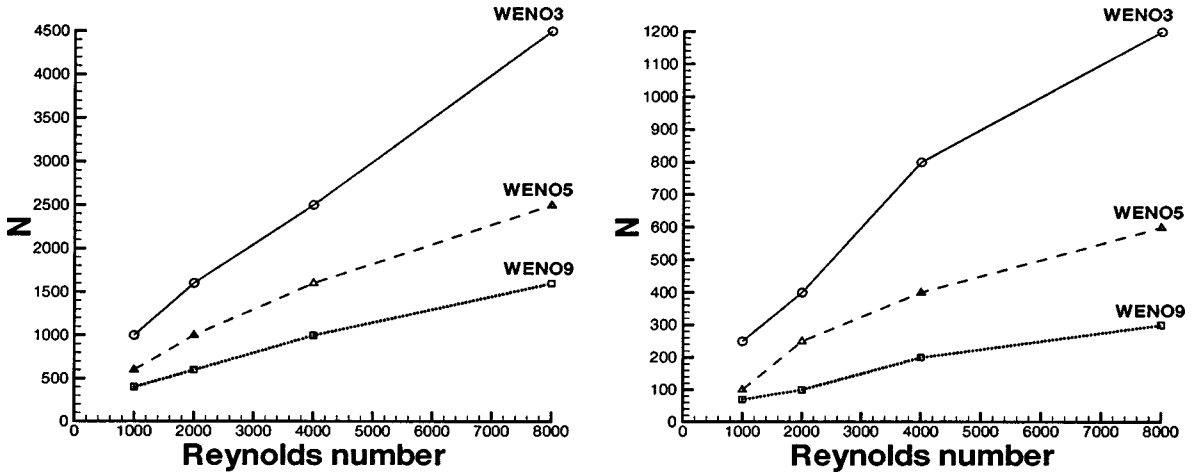

FIG. 7. The relationship of the numerical viscosity of WENO schemes and the physical viscosity of the Navier-Stokes equations, in the shock region (left) and in the contact discontinuity region (right). The *x* axis is the Reynolds number whose reciprocal is the physical viscosity, and the *y* axis is the number of grid points *N* used in the WENO schemes. The solid line with circles is for the third-order WENO, the dashed line with triangles is for the fifth-order WENO, and the dotted line with squares is for the ninth-order WENO.

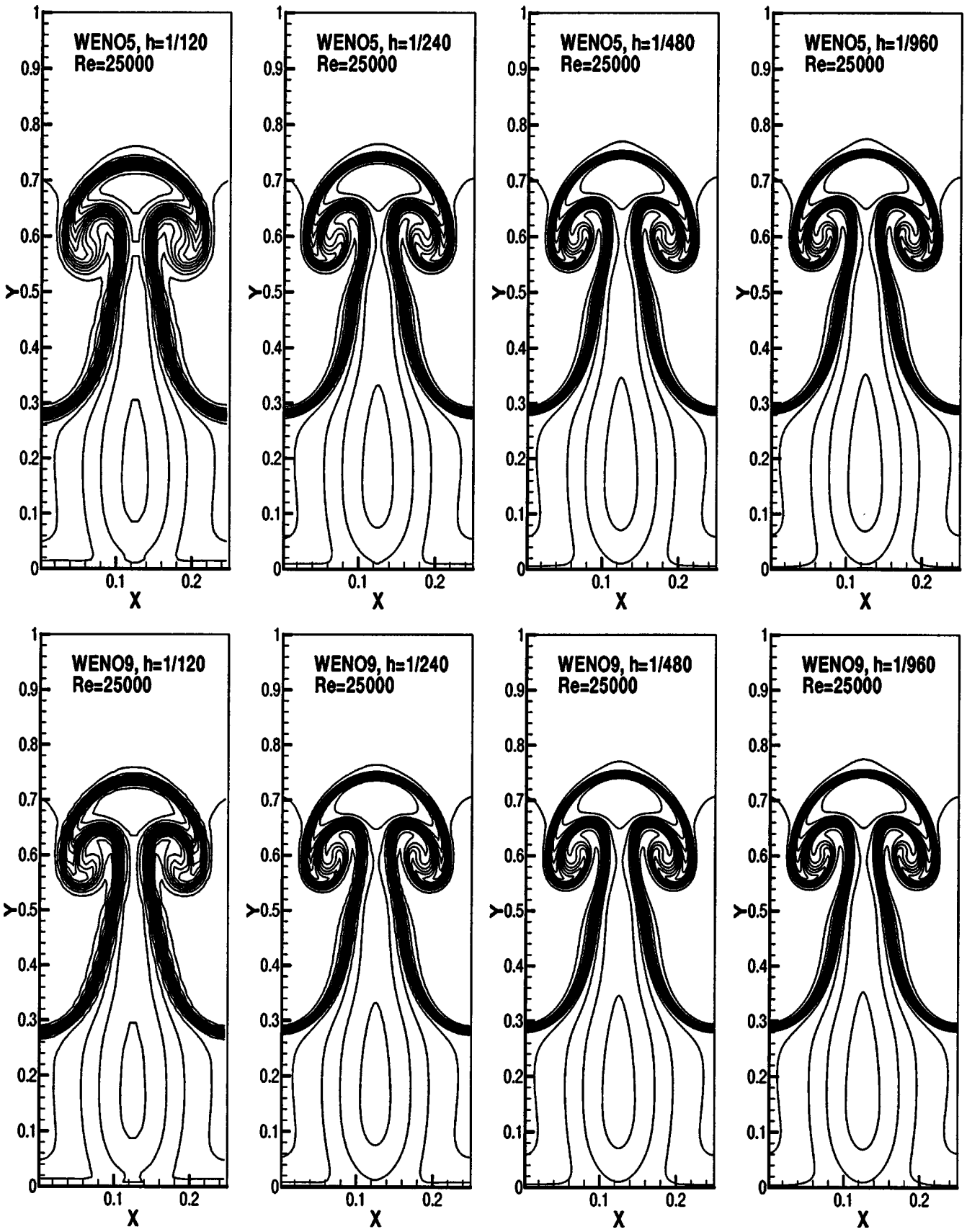

FIG. 8. Rayleigh-Taylor instability. Reynolds number$=25\,000$. Density ρ; 15 equally spaced contour lines from $\rho=0.952\,269$ to $\rho=2.145\,89$. Top from left to right: fifth-order WENO results with $h=\frac{1}{120},\frac{1}{240},\frac{1}{480},\frac{1}{960}$; bottom from left to right: ninth-order WENO results with $h=\frac{1}{120},\frac{1}{240},\frac{1}{480},\frac{1}{960}$.

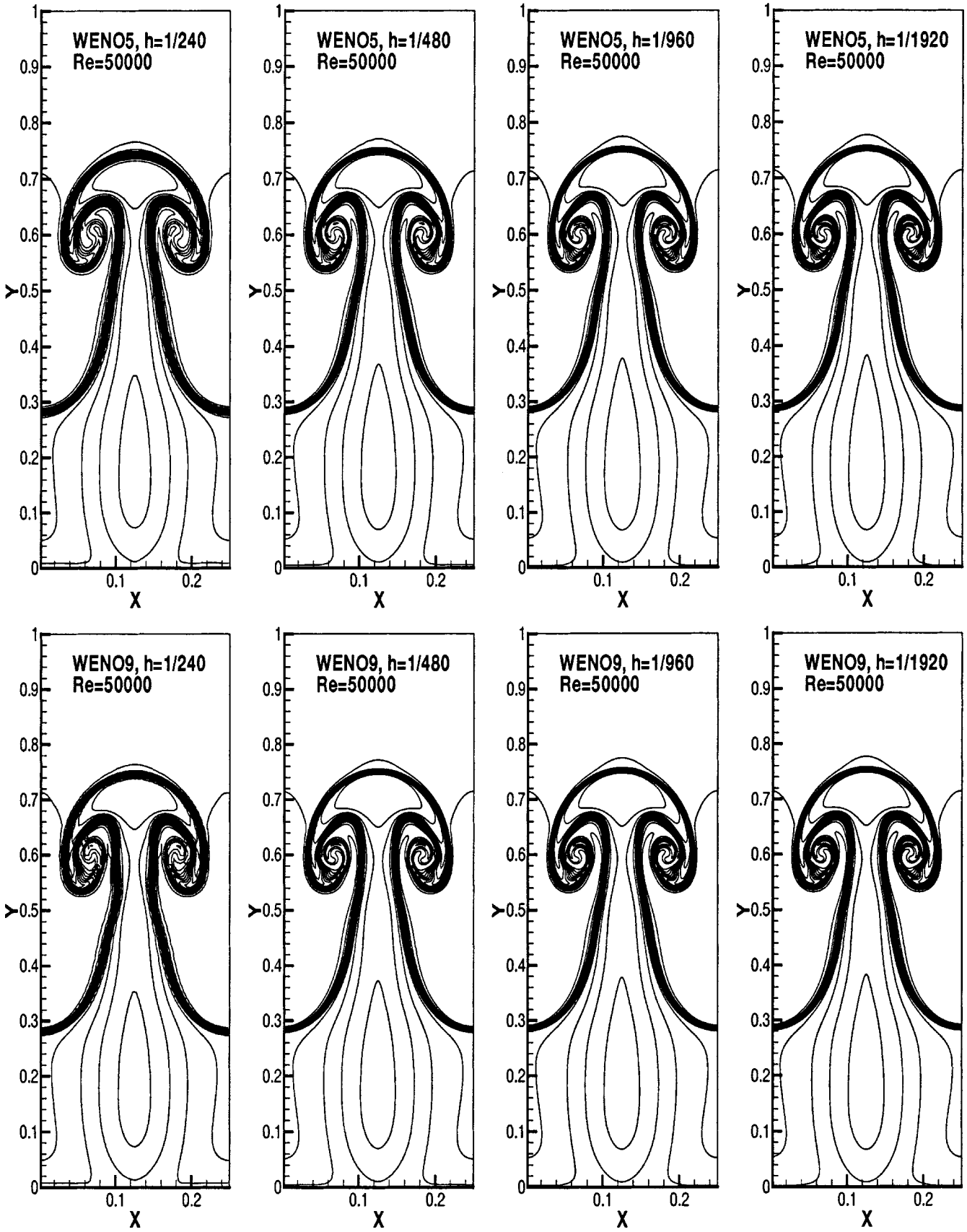

FIG. 9. Rayleigh-Taylor instability. Reynolds number$=50\,000$. Density ρ; 15 equally spaced contour lines from $\rho=0.952\,269$ to $\rho=2.145\,89$. Top from left to right: fifth-order WENO results with $h=\frac{1}{240},\frac{1}{480},\frac{1}{960},\frac{1}{1920}$; bottom from left to right: ninth-order WENO results with $h=\frac{1}{240},\frac{1}{480},\frac{1}{960},\frac{1}{1920}$.

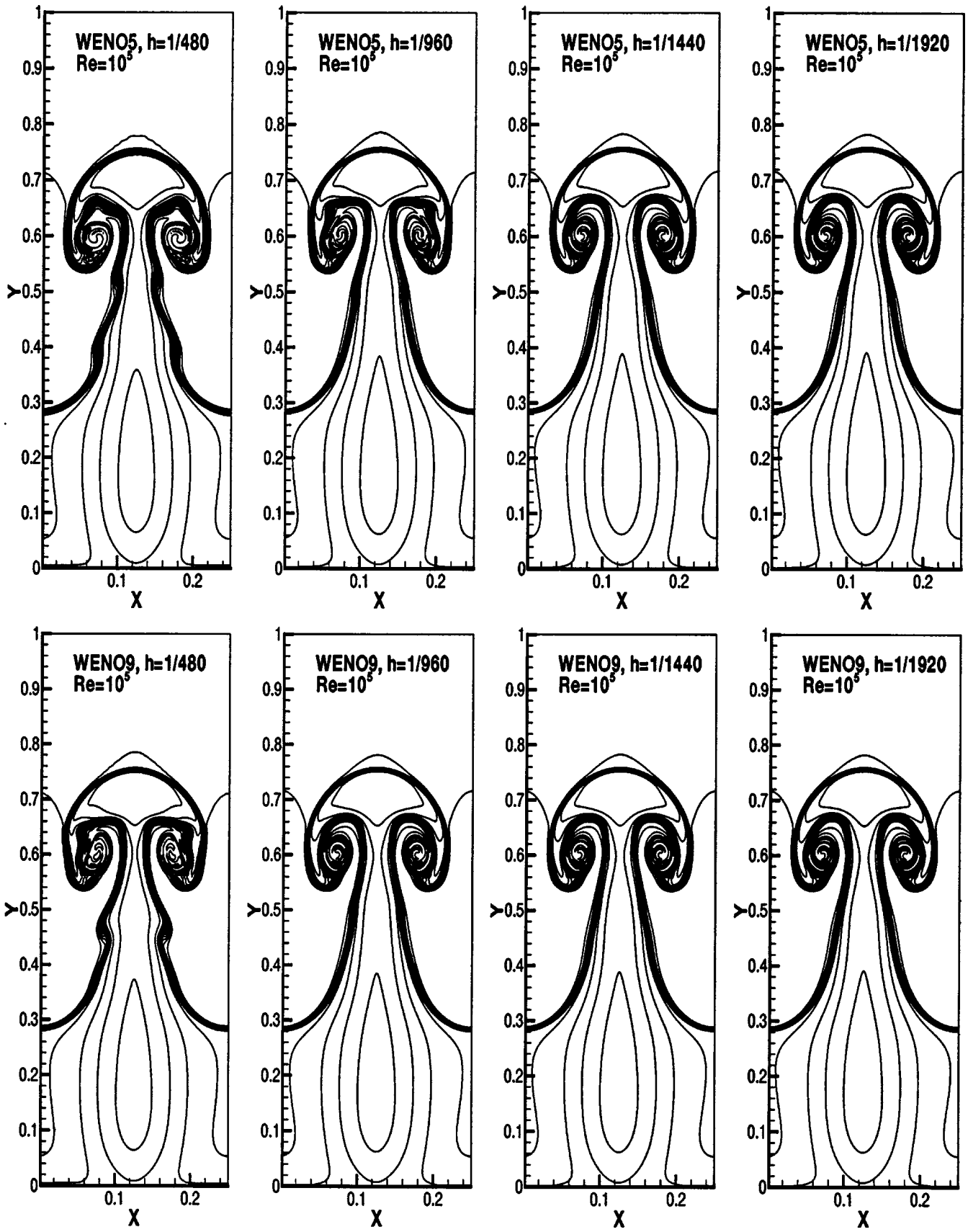

FIG. 10. Rayleigh-Taylor instability. Reynolds number $=10^5$. Density ρ; 15 equally spaced contour lines from $\rho=0.952\,269$ to $\rho=2.145\,89$. Top from left to right: fifth-order WENO results with $h=\frac{1}{480},\frac{1}{960},\frac{1}{1440},\frac{1}{1920}$; bottom from left to right: ninth-order WENO results with $h=\frac{1}{480},\frac{1}{960},\frac{1}{1440},\frac{1}{1920}$.

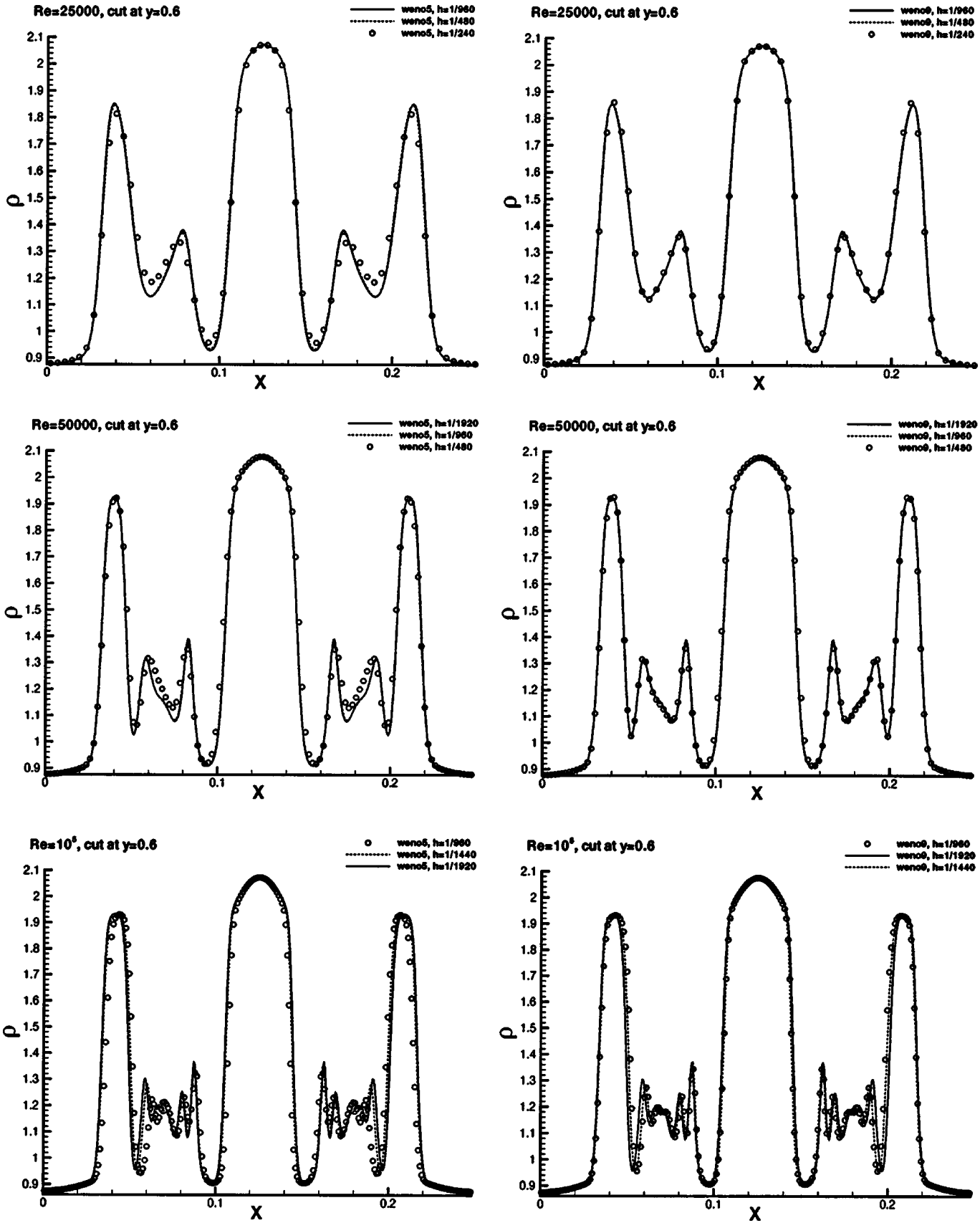

FIG. 11. Rayleigh-Taylor instability. Density ρ, 1D cut at $y=0.6$ for numerical results with different mesh sizes. Left: fifth-order WENO scheme; right: ninth-order WENO scheme. Top: Re=25 000; middle: Re=50 000; bottom: Re=10^5.

TABLE VII. Mesh size threshold values h to obtain resolved solutions. Rayleigh-Taylor instability.

Reynolds no.	h of WENO5	h of WENO9
25 000	1/480	1/240
50 000	1/960	1/480
100 000	1/1440	1/960

fifth-, and ninth-order WENO schemes, using the one-dimensional test case in the previous subsection. In other words, we attempt to find the corresponding ''numerical Reynolds number'' for the WENO schemes, which is of course a function of the number of grid points.

First we compute the ''converged'' solutions of Navier-Stokes equations with Reynolds numbers $\mathrm{Re}=10^3$, 2×10^3, 4×10^3, 8×10^3 using fifth-order WENO schemes with an adequately large number of grid points, with absolute and relative L^1 asymptotic convergence errors (see definition 1.1) to be less than 10^{-3}. We use these converged solutions as ''exact solutions'' of the Navier-Stokes equations and the viscosities of these solutions as the physical viscosities. We then try to match these ''exact solutions'' of the Navier-Stokes equations with the numerical solutions of Euler equations using the third-order, fifth-order, or the ninth-order WENO schemes (denoted by WENO3, WENO5, and WENO9), and try to find the grid point number N with which the WENO solution of the Euler equations matches the ''exact solution'' of the Navier-Stokes equations with one of those Reynolds numbers. Of course, since the numerical viscosities are of a different format from the physical viscosities, this match cannot be exact. A more accurate description is to find the grid point number N with which the L^1 absolute difference between the WENO solution of the Euler equations and the ''exact solution'' of the Navier-Stokes equations with one of those Reynolds numbers is as small as possible. It turns out that this is possible only if we isolate the shocked region from the contact discontinuity region, because the ability of the grid number N to achieve this match is different in these two cases.

We plot the matching pictures for the WENO5 case in Figs. 5 and 6. The situations for the WENO3 and WENO9 cases are qualitatively similar, hence the graphs are omitted. In Fig. 5 we try to find the grid point number N for the numerical solution of the Euler equations to match the ''exact solution'' of the Navier-Stokes equations at the bottom of the left shock in the pressure solution, and in Fig. 6 we try to find them to match at the bottom of the contact discontinuity of the density solution. These matchings are within an L^1 relative difference of less than 4%.

We summarize the results as follows.

(i) It is impossible to match well (within 5% L^1 relative error) the numerical solution of the Euler equations with the ''exact solution'' of the Navier-Stokes equations everywhere in the computational domain. This is because the exact form of the numerical viscosity is different from that of the physical viscosity, hence their ratio is not a constant throughout the computational domain. In Fig. 5 we can see that if we match them at the left shock, we cannot match them at the right shock. We cannot even match the bottom and the top of the left shock of the pressure solution at the same time. So we have to concentrate on matching them at a small local area. We obtain our matching results at the bottom part of the left shock of the pressure solution. The same thing happens for the contact discontinuity. In Fig. 6 we cannot match the bottom and the top of the contact discontinuity at the same time, so we obtain our N by matching them at the bottom part of the contact discontinuity.

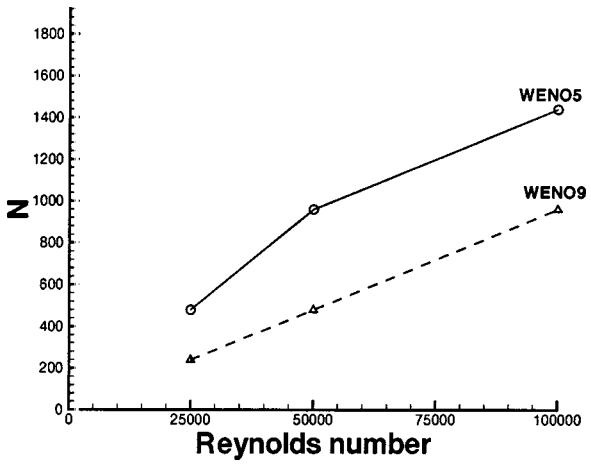

FIG. 12. The relationship of the Reynolds number and the number of mesh points in the y direction. Rayleigh-Taylor flow. The x axis is the Reynolds numbers, and the y axis is the threshold number of grid points in the y direction that WENO uses. The solid line with circles is for the fifth-order WENO; the dashed line with triangles is for the ninth-order WENO.

(ii) We find the number of grid points N for the numerical solution of the Euler equations to match as well as possible (within 5% L^1 relative error) the ''exact solutions'' of the Navier-Stokes equations with certain Reynolds numbers, and list this correspondence in Table V for the shock case and in Table VI for the contact discontinuity case, with the third-, fifth-, and ninth-order WENO schemes. We also plot the relationship of this Reynolds number versus the number of grid points N in Fig. 7 for the shock case (left) and for the contact discontinuity case (right). We can see that, for a WENO scheme of a given order, this relationship is almost linear. However, higher-order WENO schemes have much higher ''numerical Reynolds numbers'' than the lower-order ones for the same number of grid points N.

(iii) From Tables V and VI and Fig. 7, we can compare the numerical viscosities of the third-, fifth-, and ninth-order WENO schemes. The conclusion is that the numerical viscosity of the third-order WENO scheme is almost twice that of the fifth-order WENO scheme, because for the same N ($N=1000,1600,2500$ for the shock or $N=250,400$ for the contact discontinuity), the corresponding Reynolds number of the third-order WENO scheme is about one-half of the fifth-order one. The same is true for the fifth-order WENO scheme versus the ninth-order one, i.e., the numerical viscosity of WENO5 is almost twice that of WENO9.

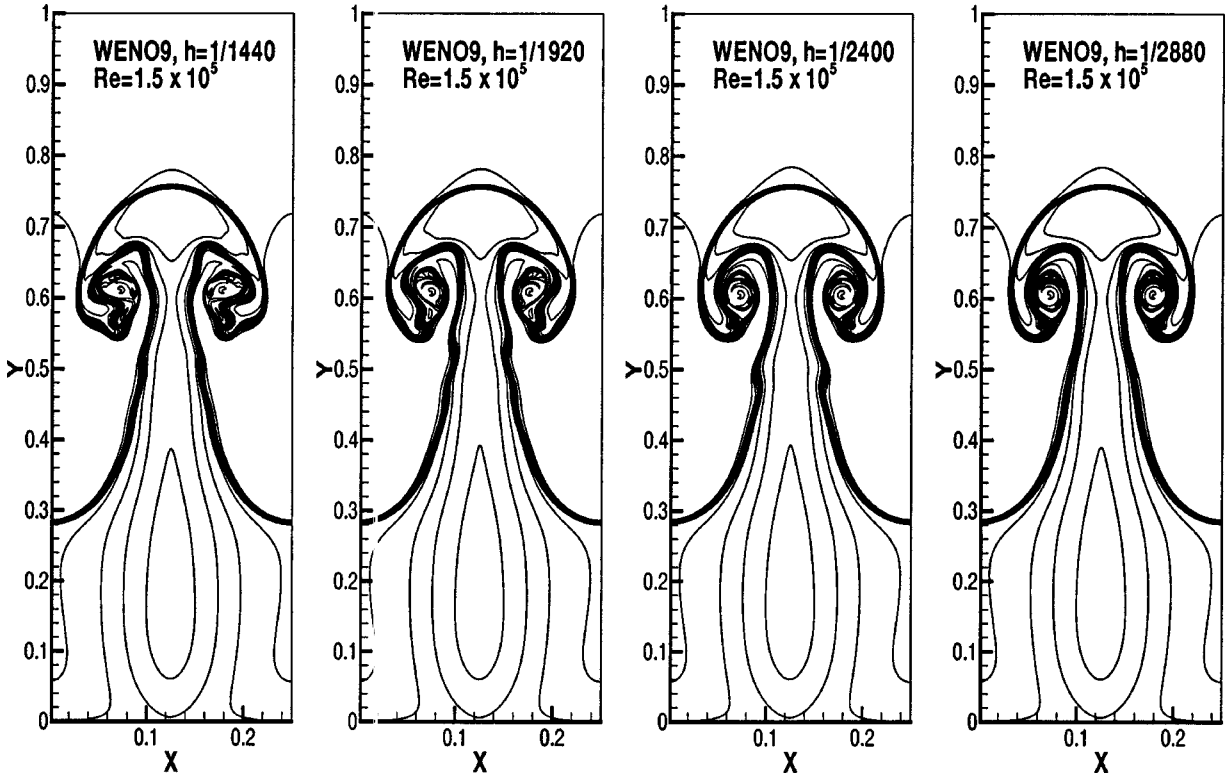

FIG. 13. Rayleigh-Taylor instability problem. Ninth-order WENO scheme. Density ρ; 15 equally spaced contour lines from $\rho = 0.952\,269$ to $\rho = 2.145\,89$. $\mathrm{Re} = 1.5 \times 10^5$. From left to right: $h = \frac{1}{1440}$, $\frac{1}{1920}$, $\frac{1}{2400}$, and $\frac{1}{2880}$. The rightmost result with $h = \frac{1}{2880}$ is a resolved solution verified by further grid refinement.

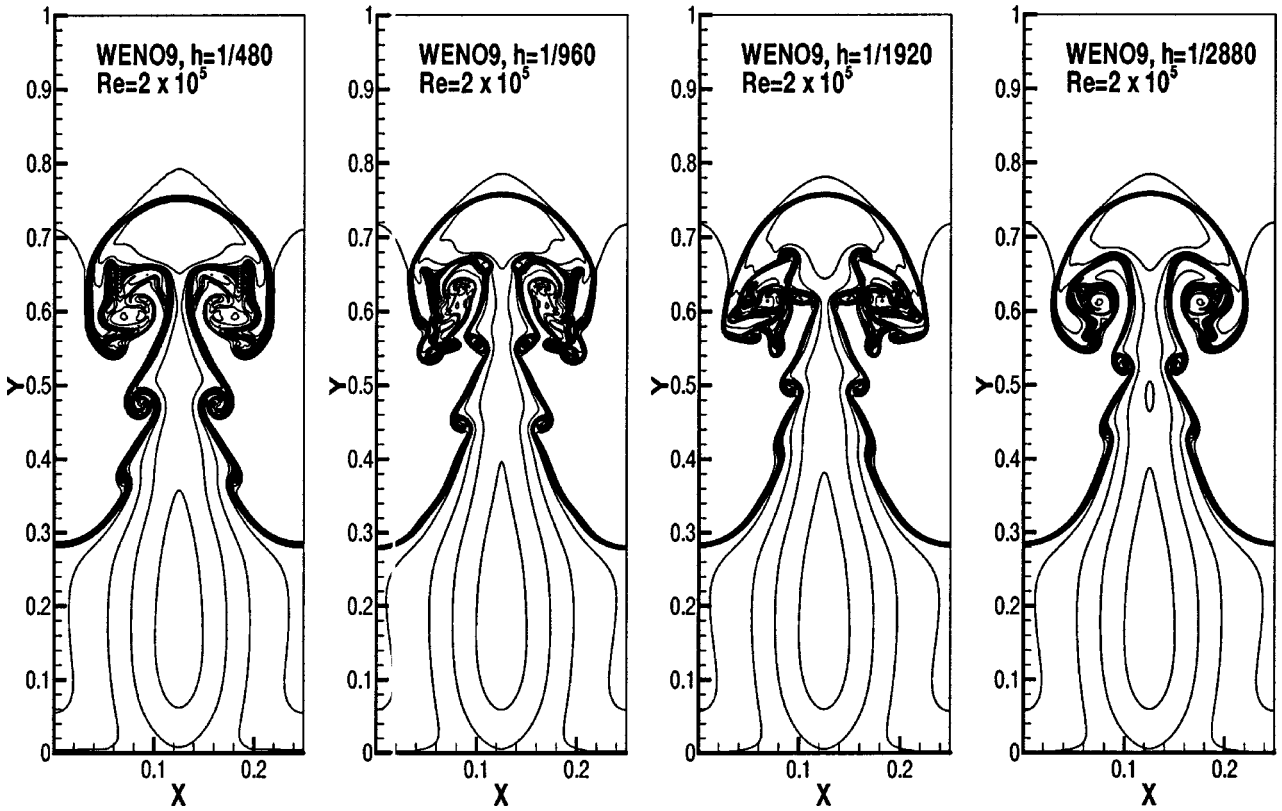

FIG. 14. Rayleigh-Taylor instability. Ninth-order WENO scheme. Reynolds number $= 2 \times 10^5$. Density ρ; 15 equally spaced contour lines from $\rho = 0.952\,269$ to $\rho = 2.145\,89$. From left to right: $h = \frac{1}{480}, \frac{1}{960}, \frac{1}{1920}, \frac{1}{2880}$.

III. THE TWO-DIMENSIONAL RAYLEIGH-TAYLOR FLOW

Now we consider the two-dimensional nondimensionalized Navier-Stokes equations with a gravitation source term:

$$\rho_t+(\rho u)_x+(\rho v)_y=0,$$

$$(\rho u)_t+(\rho u^2+p)_x+(\rho uv)_y=\frac{1}{\mathrm{Re}}\left(\frac{4}{3}u_{xx}+u_{yy}+\frac{1}{3}v_{xy}\right),$$

$$(\rho v)_t+(\rho uv)_x+(\rho v^2+p)_y=\frac{1}{\mathrm{Re}}\left(v_{xx}+\frac{4}{3}v_{yy}+\frac{1}{3}u_{xy}\right)+\rho,$$

$$E_t+[u(E+p)]_x+[v(E+p)]_y=\frac{1}{\mathrm{Re}}\left(\frac{2}{3}(u^2)_{xx}-\frac{2}{3}(uv_y)_x+\frac{1}{2}(v^2)_{xx}+(vu_y)_x+\frac{1}{2}(u^2)_{yy}+(uv_x)_y+\frac{2}{3}(v^2)_{yy}-\frac{2}{3}(vu_x)_y\right.$$
$$\left.+\frac{1}{(\gamma-1)\mathrm{Pr}}[(C^2)_{xx}+(C^2)_{yy}]\right)+\rho v, \tag{8}$$

where ρ is the density, (u,v) is the velocity, E is the total energy, and p is the pressure, related to the total energy by $E=[p/(\gamma-1)]+\frac{1}{2}\rho(u^2+v^2)$ with the ratio of specific heats γ being a constant. C is the sound speed and $C^2=\gamma p/\rho$. Re is the Reynolds number. $\mathrm{Pr}=0.7$ is the Prandtl number.

We perform the numerical simulation for 2D Rayleigh-Taylor flow with the Navier-Stokes equations (8). Rayleigh-Taylor instability happens on an interface between fluids with different densities when an acceleration is directed from the heavy fluid to the light fluid. The instability has a fingering nature, with bubbles of light fluid rising into the ambient heavy fluid and spikes of heavy fluid falling into the light fluid; see, for example, [16] and [17]. Small-scale features are generated by this instability. If the Euler equations are solved, then the size and specific shapes of these small-scale features are dependent on the numerical schemes and the mesh sizes; see, for example [7] for the results obtained with the high-order WENO schemes and [18] for the results obtained with the discontinuous Galerkin method using an adaptive mesh.

While Euler simulations are important to identify the size of the numerical viscosities and to demonstrate the onset of the small-scale features, the specific shape and growth of these small features obtained by an Euler equation simulation is not reliable, as they are driven by the numerical viscosities of the schemes, not by the physical viscosities of the Navier-Stokes equations.

In this section, we attempt to simulate the Navier-Stokes equations (8) directly with resolved numerical solutions using high-order WENO schemes. The onset, shapes, and growth of the small-scale features obtained this way are reliable, since they are driven by the physical viscosities in the Navier-Stokes equations. We also compare the resolution power of the fifth- and ninth-order WENO schemes for such simulations.

We set up the problem as follows: the computational domain is $[0,\frac{1}{4}]\times[0,1]$; initially the interface is at $y=\frac{1}{2}$, the heavy fluid with density $\rho=2$ is below the interface, and the light fluid with density $\rho=1$ is above the interface with the acceleration in the positive y direction; the pressure p is continuous across the interface; a small perturbation is given to the y-direction fluid speed, thus for $0\leqslant y<\frac{1}{2}$, $\rho=2$, $u=0$, $p=2y+1$, and $v=-0.025C\cos(8\pi x)$; and for $\frac{1}{2}\leqslant y\leqslant 1$, $\rho=1$, $u=0$, $p=y+\frac{3}{2}$, and $v=-0.025C\cos(8\pi x)$, where C is the sound speed, $C=\sqrt{\gamma p/\rho}$, and the ratio of specific heats $\gamma=\frac{5}{3}$; reflective boundary conditions are imposed for the left and right boundaries; at the top boundary, the flow values are set as $\rho=1$, $p=2.5$, $u=v=0$, and at the bottom boundary they are $\rho=2$, $p=1$, $u=v=0$; the source term ρ is added to the right-hand side of the third equation and ρv is added to the fourth equation of the Navier-Stokes system (8). The final simulation time is $t=1.95$.

The fifth-order finite-difference WENO scheme (WENO5) [9] associated with a fourth-order central approximation to the viscous terms, and the ninth-order WENO scheme (WENO9) [10] associated with an eighth-order central approximation to the viscous terms, are used. The two-dimensional computations reported in this paper are performed on the IBM SP parallel computer using up to 72 processors at the Technology Center for Advanced Scientific Computing and Visualization of Brown University. The parallel efficiency is over 90% when the operation per processor is kept constant, i.e., when the number of processors increases together with a mesh refinement.

We first compute the cases of $\mathrm{Re}=2.5\times10^4$, 5×10^4, 10^5, and look for mesh size threshold values to get converged solutions for different Reynolds numbers, using WENO5 and WENO9. We do the convergence study and refine the mesh continuously. The numerical results with different mesh sizes are shown in Figs. 8–10. We also present the cut of the numerical results at $y=0.6$ in Fig. 11, where the solutions have the richest structures, to observe visually the convergence of the numerical solutions.

We list the mesh size threshold values to obtain resolved solutions for $\mathrm{Re}=2.5\times10^4$, 5×10^4, 10^5 in Table VII. Resolved solutions are measured by the absolute asymptotic

convergence errors, as defined in definition 1.1, to be less than 0.01 (the relative asymptotic errors are at the same levels). In Fig. 12, we plot the relationship of the Reynolds number and the threshold mesh point number $N=1/h$ in the y direction. We can conclude that the relationship is almost linear. To obtain resolved solutions at the same level, WENO5 needs twice as many grid points in each direction as WENO9.

Next we show in Fig. 13 the simulation results for the Reynolds number $\mathrm{Re}=1.5\times10^5$ using WENO9 on four different meshes, with 360×1440, 480×1920, 600×2400, and 720×2880 uniformly spaced mesh points, respectively (from left to right). We can see that there are noticeable differences in the details of the solutions at these four mesh levels, indicating that even at the mesh of 600×2400 points the solution is still not a resolved solution. The result in the right picture using the 720×2880 mesh is a resolved solution verified by a further grid refinement study using a 900×3600 mesh, with an L^1 absolute difference between these two meshes being less than 4×10^{-3}. The small-scale structures in the resolved solutions should be reliable as they are driven by physical rather than numerical viscosities.

Finally, we present the simulation results for $\mathrm{Re}=2\times10^5$ in Fig. 14, which appear to be a mixture of resolved and under-resolved features. The small structures in the final figure are still not faithful since there are visually noticeable differences among all graphs shown in Fig. 14. The L^1 absolute difference between the solutions of the two rightmost graphs in Fig. 14 is at the level of 4×10^{-2}.

IV. CONCLUDING REMARKS

In this paper, we have attempted to quantitatively study the size of numerical viscosities, or numerical Reynolds numbers, of high-order WENO (weighted essentially nonoscillatory) third-, fifth-, and ninth-order schemes. It seems that such numerical viscosities decrease linearly with the mesh size for WENO with a given order of accuracy. For a fixed mesh, the numerical viscosity of a fifth-order WENO is about half that of a third-order WENO and that of a ninth-order WENO is about half that of a fifth-order WENO. Thus, it would imply a reduction factor of $4^3=64$ space-time grid points in 2D to use WENO9 rather than WENO3 to obtain the same numerical viscosity and the same resolution. This improves the computational efficiency tremendously. The high-order WENO schemes also have excellent parallel efficiency. A one-dimensional shock tube problem, a one-dimensional example motivated by the supernova and laser experiments, and a two-dimensional Rayleigh-Taylor instability problem are used for the numerical tests. It is argued that the only reliable small-scale features in such solutions are those driven by the physical rather than the numerical viscosities, hence high-order WENO schemes are advantageous because they provide resolved solutions for the Navier-Stokes equations at much coarser meshes than the lower-order schemes.

ACKNOWLEDGMENTS

The authors are very grateful to Dr. O. Hurricane for providing his laser simulation data reported in Ref. [14]. The research of Y.-T. Zhang was partially supported by ARO Grant No. DAAD19-00-1-0405 and NSF Grant No. DMS-9804985. The research of C.-W.S. was partially supported by LLNL Subcontract No. B513236, ARO Grant No. DAAD19-00-1-0405, NSF Grant No. DMS-0207451, NASA Langley Grant No. NCC1-01035, and AFOSR Grant No. F49620-02-1-0113. The research of Y.Z. was performed under the auspices of the U.S. Department of Energy by the University of California Lawrence Livermore National Laboratory under Contract No. W-7405-Eng-48.

[1] B. A. Remington, D. Arnett, R. P. Drake, and H. Takabe, Science **284**, 1488 (1999).
[2] B. A. Remington, R. P. Drake, H. Takabe, and D. Arnett, Phys. Plasmas **7**, 1641 (2000).
[3] L. D. Landau and E. M. Lifshitz, *Fluid Mechanics* (Pergamon, Oxford, 1987).
[4] S. Chandrasekhar, *Hydrodynamic and Hydromagnetic Stability* (Dover, New York, 1961).
[5] Lord Rayleigh, *Scientific Papers. Volume 2* (Cambridge University Press, Cambridge, UK, 1900).
[6] G. I. Taylor, Proc. R. Soc. London, Ser. A **201**, 192 (1950).
[7] J. Shi, Y.-T. Zhang, and C.-W. Shu, J. Comput. Phys. **186**, 690 (2003).
[8] X.-D. Liu, S. Osher, and T. Chan, J. Comput. Phys. **115**, 200 (1994).
[9] G. Jiang and C.-W. Shu, J. Comput. Phys. **126**, 202 (1996).
[10] D. Balsara and C.-W. Shu, J. Comput. Phys. **160**, 405 (2000).
[11] C.-W. Shu, *Essentially Non-oscillatory and Weighted Essentially Non-oscillatory Schemes for Hyperbolic Conservation Laws*, in B. Cockburn, C. Johnson, C.-W. Shu, and E. Tadmor, *Advanced Numerical Approximation of Nonlinear Hyperbolic Equations*, edited by A. Quarteroni, Lecture Notes in Mathematics Vol. 1697 (Springer, Berlin, 1998), pp. 325–432.
[12] C.-W. Shu and S. Osher, J. Comput. Phys. **77**, 439 (1988).
[13] D. Ryutov, R. P. Drake, J. Kane, E. Liang, B. A. Remington, and W. M. Woodvasey, Astrophys. J. **518**, 821 (1999).
[14] R. P. Drake, H. F. Robey, O. A. Hurricane, Y. Zhang, B. A. Remington, J. Knauer, J. Glimm, D. Arnett, J. O. Kane, K. S. Budil, and J. Grove, Astrophys. J. **564**, 896 (2002).
[15] H. Robey, Y. Zhou, A. Buckingham, R. P. Drake, B. A. Remington, and P. Keiter, Phys. Plasmas **10**, 614 (2003).
[16] C. L. Gardner, J. Glimm, O. McBryan, R. Menikoff, D. H. Sharp, and Q. Zhang, Phys. Fluids **31**, 447 (1988).
[17] Y.-N. Young, H. Tufo, A. Dubey, and R. Rosner, J. Fluid Mech. **447**, 377 (2001).
[18] J.-F. Remacle, J. E. Flaherty, and M. S. Shephard, SIAM Rev. **45**, 53 (2003).